

Fine Adjustment of Interfacial Potential between pH-Responsive Hydrogels and Cell-Sized Particles

Cornelia Monzel,^{†,‡} Mariam Veschgini,[†] Jeppe Madsen,[‡] Andrew L. Lewis,[§] Steven P. Armes,[‡] and Motomu Tanaka^{*,†,||}

[†]Physical Chemistry of Biosystems, Institute of Physical Chemistry, University of Heidelberg, 69120 Heidelberg, Germany

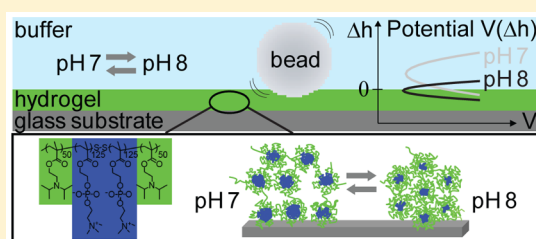
[‡]Department of Chemistry, Dainton Building, University of Sheffield, Brook Hill, Sheffield, South Yorkshire, S3 7HF, United Kingdom

[§]Biocompatibles UK, Ltd., Chapman House, Farnham Business Park, Weydon Lane, Farnham, Surrey GU9 8 QL, United Kingdom

^{||}Institute for Integrated Cell-Material Sciences (WPI iCeMS), Kyoto University, 606-8501, Kyoto, Japan

Supporting Information

ABSTRACT: We quantitatively determined interfacial potentials between cell-sized particles and stimulus-responsive hydrogels using a microinterferometer. The hydrogel is based on physically interconnected ABA triblock copolymer micelles comprising an inner biocompatible PMPC block and two outer pH-responsive PDPA blocks. The out-of-plane temporal fluctuation in the position of the cell-sized particles was calculated from changes in the interference pattern measured by Reflection Interference Contrast Microscopy (RICM), thus yielding the particle-substrate interaction potential V (Δh). Measurements in pH buffers ranging from 7.0 to 7.8 resulted in a systematic reduction in height of the potential minima $\langle \Delta h \rangle$ and a concomitant increase in the potential curvature V'' (Δh). The experimental data were analyzed by applying the modified Ross and Pincus model for polyelectrolytes, while accounting for gravitation, lubrication and van der Waals interactions. Elastic moduli calculated from V'' (Δh) were in good agreement with those measured by Atomic Force Microscopy. The ability to fine-tune both the gel elasticity and the interfacial potential at around physiological pH makes such triblock copolymer hydrogels a promising biocompatible substrate for dynamic switching of cell–material interactions.



INTRODUCTION

During the past decade stimulus-responsive polymers have been the subject of increasing attention. Since their physical characteristics can be changed dynamically and some of them exhibit properties such as biocompatibility and high resistance to corrosion and biofouling, these polymers are anticipated to cover a wide range of biomedical applications.^{1–5} In the past, several successful approaches for medical therapeutics using static polymer systems have been reported, including the development of implants with controlled hydrolytic degradation profiles based on poly(lactic acid),^{6,7} surgical stents, or extended-wear contact lenses.^{8–10} More recently, dynamically tunable polymers have been designed that are capable of responding to artificial triggers and biological signals.¹¹ For example, thermoresponsive poly(*N*-isopropylacrylamide)-based hydrogels have been utilized by Okano and co-workers to support the formation of two-dimensional cell sheets which are readily used for transplantation.^{12,13} DeForest and Anseth designed click-based hydrogels which enable dynamic orthogonal stem cell entrapment and recovery,¹⁴ while Zhao et al. reported on polyaniline-based conductive polymer hydrogels for use in drug delivery and glucose sensor devices.¹⁵

Adaptable hydrogels have recently attracted considerable interest due to their ability to model the highly dynamic cellular

environment. For example, studies by Discher, Engler and Vogel provided compelling evidence of how cells sensitively react to changes in their micromechanical environment.^{7,16,17} Degeneration of alginate scaffolds in vivo enables enhanced bone regeneration by transplanted stem cells,¹⁸ stiffening of liver cells was suggested to be a consequence of fibrosis,¹⁹ and various characteristics in cancer cell migration were observed as a response to matrix density changes during invasion.²⁰ In vitro models of the extracellular matrix (ECM) based on chemically cross-linked hydrogels have been shown to play a crucial role in various cellular processes, including effects on cell morphology^{21–23} and motility of contractile cells^{24,25} as well as the differentiation of mesenchymal stem cells.^{7,16}

Most literature studies rely on *ex situ* control of substrate stiffness using chemical cross-linkers^{26–28} and the irreversible formation or destruction of disulfide bonds formed therein. However, since cellular sensing processes are highly dynamic, the cell response toward time-dependent mechanical stresses requires monitoring.¹¹ For example, we recently reported using a physically cross-linked biocompatible hydrogel composed of

Received: May 22, 2015

Revised: July 9, 2015

Published: July 19, 2015

interconnected triblock copolymer micelles whose gel elasticity could be conveniently modulated using subtle changes in pH to demonstrate reversible switching in mechanosensing by cardiac myoblast cells (C2C12).²⁹ This triblock copolymer, which is also the basis of the present study, consists of a central B block of poly-2-methacryloyloxyethyl phosphorylcholine (PMPC, mean degree of polymerization, $n = 250$) and two outer A blocks composed of poly-2-(diisopropylamino)ethyl methacrylate (PDPA, $n = 50$ for each).³⁰ PDPA is a weak polyelectrolyte (the pK_a of protonated PDPA homopolymer is around pH 6.2) which shows distinct changes in its mean degree of ionization close to physiological pH, while PMPC confers excellent biocompatibility. In our previous study, the hydrogel elasticity was tuned by exchanging cell culture media of various pH over 3 h intervals and a corresponding reversible response of C2C12 cells was observed. On relatively stiff substrates, these cells adopted a stretched, flattened morphology, but less elongated, rounded cells, along with a 2-fold reduction in cell adhesion strength, were obtained on softer hydrogels. Changes in the mechanical environment quickly triggered discernible changes in cell morphology (within ~ 10 min) and no significant time lag in the cellular response was observed.

However, to date, the physical properties of this biocompatible triblock copolymer hydrogel have been discussed mostly in terms of its bulk elastic modulus (Young's modulus) as measured by nanoindentation, and its surface properties are largely uncharacterized. As this is likely to be important for specific biomedical applications, herein we utilize a noninvasive technique based on colloidal probes to quantitatively demonstrate how the interfacial potential between stimulus-responsive polymer substrates and cell-sized model latex particles can be adjusted with high precision. As schematically shown in Figure 1, the PDPA₅₀-PMPC₂₅₀-PDPA₅₀ triblock

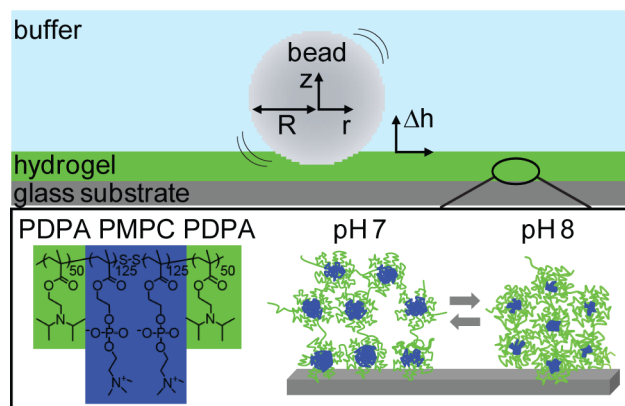


Figure 1. Schematic view of the experiment. A polystyrene latex particle is fluctuating at a distance Δh above the triblock polymer hydrogel. The magnified sketch illustrates the structure of PDPA₅₀-PMPC₂₅₀-PDPA₅₀ hydrogel at different buffer pH. Note the drawing is not to scale.

copolymer used in this study forms a soft hydrogel at around pH 7, while deprotonation of the PDPA blocks results in a relatively stiff hydrogel at pH 8.³¹ To assess whether interfacial interactions with cell-sized objects could be regulated by pH modulation, we monitor the height fluctuations of a latex particle above the hydrogel by means of Reflection Interference Contrast Microscopy (RICM) and analyze the particle-gel interactions in detail.

EXPERIMENTAL SECTION

Materials. Ultrapure water from a water purification system (TKA, Niederelbert, Germany) was used throughout this study. HEPES buffer solution containing 10 mM 4-(2-hydroxyethyl)-1-piperazine ethane sulfuric acid and 150 mM sodium chloride was adjusted in pH between 7.0 to 8.0 in steps of 0.2 by adding HCl or KOH. Chemicals for buffers were purchased from Carl Roth (Karlsruhe, Germany) or Sigma-Aldrich (St. Louis, MO, U.S.A.) and used without further purification. Latex particles (Macherey-Nagel, Düren, Germany) of 10 μm radius and 1.05 g/cm^3 density were preincubated in 1 mg/mL Bovine Serum Albumin (BSA, Carl Roth) solution for 15 min prior to addition to the measurement chamber. The BSA layer was necessary to prevent unspecific interaction of the particle with the substrate.

Synthesis of PDPA₅₀-PMPC₂₅₀-PDPA₅₀ triblock copolymer was reported before and is briefly described in the Supporting Information (SI(1)).^{31–33}

Sample Preparation. For preparation of triblock copolymer hydrogel substrates, glass slides ($24 \times 24 \text{ mm}^2$, Carl Roth) were cleaned with a so-called modified RCA protocol.³⁴ As previously reported,²⁹ PDPA₅₀-PMPC₂₅₀-PDPA₅₀ was deposited onto a glass substrate by spin-coating for 60 s at 4000 rpm from a methanolic solution (50 mg/mL). Each sample was annealed at 80 $^\circ\text{C}$ under nitrogen flow for 1 h, and dried overnight in a vacuum oven at 80 $^\circ\text{C}$. Thirty min prior to the experiment, samples were immersed in buffer and particles were added to equilibrate to ambient conditions. This way the lateral drift of the particles hovering over the hydrogel was minimized.

RICM. RICM images of particle fluctuations were recorded with an inverted microscope (Axiovert200, Zeiss, Germany), equipped with an oil immersion objective (NA 1.25, 63x, PH3). The light source consisted of a high-pressure metal halide lamp of which the 546 nm wavelength was selected from the spectrum with a bandpass filter. To achieve images of high contrast, the Antiflex Technique was applied. Therefore, 2 polarizers of perpendicular orientation were inserted into the light path. One was placed in the illumination and one in the detection light path. In addition, a quarter-wave plate located behind the front lens of the objective was used. The Illumination Numerical Aperture (INA) was adjusted with the aperture diaphragm and minimized to its smallest value of 0.48 to record many interference orders.³⁵ Images were detected with a CCD camera (Orca-1ER, Hamamatsu Photonics, Hamamatsu, Japan). 1000 consecutive images were recorded at an exposure time of 30 ms.

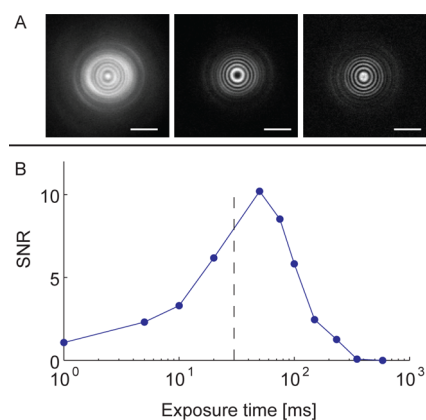


Figure 2. Optimal settings for recording the height fluctuations of a latex particle: (A) Effect of the Illumination Numerical Aperture (INA) on the fringe pattern of the particle. At high INA = 0.8 (left) the fringe pattern is hardly visible, for intermediate INA = 0.56 the contrast improves (middle) and for INA = 0.48 (right), the highest number of fringes are discernible. Scale bar 8 μm . (B) Signal-to-noise ratio (SNR) versus camera exposure time. The SNR exhibits reasonable high values within the interval 20–200 ms. The dashed line indicates the chosen exposure time of 30 ms.

Data Analysis. Movies of particles fluctuating above the hydrogel were corrected for remaining lateral drift using cross-correlation analysis. Interference pattern of the particle were analyzed as described before.³⁶ Briefly, the theoretical intensity-height relation, $I(\Delta h)$, for reflection at 3 interfaces (glass-hydrogel, hydrogel-buffer, buffer-particle) was calculated with the refractive indices $n_{\text{glass}} = 1.525$, $n_{\text{hydrogel}} = 1.470$,^{37,38} $n_{\text{buffer}} = 1.335$, $n_{\text{particle}} = 1.55$,³⁹ the measured INA $= n_{\text{buffer}} \sin(\alpha) = 0.48$,³⁶ and the hydrogel thickness h_0 (pH8) = 3 μm or h_0 (pH7) = 4 μm ⁴⁰ with linearly interpolated intermediate values. Subsequently, this curve was fitted with the RISM theory of finite aperture:^{35,41}

$$2I(\Delta h) = S - D \frac{\sin(y)}{y} \cos\{2kn_{\text{buffer}}(\Delta h[1 - \sin^2(\alpha/2)])\}$$

S and D are the sum and difference of the maximal and minimal intensity, and Δh is the instantaneous height of the particle, i.e., the minimum particle-hydrogel separation at each time point. $y = 2k\Delta h \sin^2(\alpha/2)$ describes the damping of the intensity-height relation due to finite aperture, where $k = 2\pi n_{\text{buffer}}/\lambda$ is the wavevector for $\lambda = 546$ nm. Particle fluctuations near the hydrogel surface, defined as $\Delta h \equiv 0$, were derived converting intensities into Δh via the first branch of the cosine function at the hydrogel-buffer interface. Repeated experiments on a single sphere resulted in an accuracy of height determination of ± 4 nm (see examples in SI(2)). All analyses were performed using self-written routines in Matlab (R2008b) and IgorPro (6.3).

Theoretical Background. The vertical Brownian motion of a colloidal particle in a potential $V(\Delta h)$ is described by the Langevin equation:

$$m \frac{\partial^2 \Delta h}{\partial t^2} + \gamma \frac{\partial \Delta h}{\partial t} + \frac{\partial V}{\partial \Delta h} = \xi \quad (1)$$

Here, m is the mass of the particle, Δh the instantaneous particle-surface distance, γ the friction coefficient, and ξ is the stochastic force of the thermal environment. The Langevin eq 1 cannot be solved analytically; however, some distinct properties of the system allow for the following approximations:

1. The particle motion is overdamped, since viscous forces dominate the particle-buffer system and the Reynolds number of the system is low: $\text{Re} = 2R((\partial \Delta h)/(\partial t)) (\rho/\eta) \approx 8 \times 10^{-10} \ll 1$. Here, ρ is the particle density, η the buffer viscosity, and R the particle radius (as validated by phase contrast microscopy images to be 10.0 ± 1.4 μm). Therefore, the inertia term in (1) can be neglected.
2. Height fluctuations $\delta h = \Delta h - \langle \Delta h \rangle \approx 30$ nm are small enough to approximate the interaction potential $V(\Delta h)$ harmonically around the equilibrium height $\langle \Delta h \rangle$:⁴²

$$V(\Delta h) = \frac{1}{2} \frac{\partial^2 V}{\partial \Delta h^2} \bigg|_{\langle \Delta h \rangle} (\Delta h - \langle \Delta h \rangle)^2 = \frac{V''}{2} \delta h^2$$

These approximations enable one to solve the simplified Langevin equation $\gamma ((\partial \Delta h)/(\partial t)) + V'' \delta h = \xi$ analytically. Within the framework of the equipartition and fluctuation-dissipation theorem, the autocorrelation function of height fluctuations (hACF) read (see SI(4) for an explicit calculation):

$$\langle \delta h(\tau) \delta h(0) \rangle \approx \frac{k_B T}{V''} e^{-V''/\gamma \tau} \text{ with the correlation time } \tau_c \approx \frac{\gamma}{V''} \quad (2)$$

and k_B and T have normal meanings. At thermal equilibrium, the ensemble of particle fluctuations follows a Boltzmann probability distribution, $P(\Delta h)$, which reflects the sphere-substrate interspace dependence of the interaction potential, $V(\Delta h)$:⁴³

$$\frac{V(\Delta h)}{k_B T} = -\ln(P(\Delta h)) + \text{const} \quad (3)$$

Thus, in the harmonic limit, the elastic constant of the potential, V'' , is easily determined from the probability function of the particle height $P(\Delta h)$ or the hACF.

Interaction Potential. In the following, we identify the major forces of $V(\Delta h)$ to obtain a theoretical model describing the experimental situation:

I. Polyelectrolyte induced forces. The microstructure of the hydrogel comprises a 3D network of interconnected "flower" micelles, where the physical entanglement of PDPA chains is modulated by the degree of ionizations under pH titration (see Figure 1).^{13,17} Since there is no theoretical description available yet for such conformation, the repulsive interaction induced by polyelectrolytes is best approximated by the classical Pincus model or the Ross-Pincus model for charged brushes.^{44,45} In case of the classical theory the standard Pincus model assumes⁴⁴

- a uniform monomer concentration c throughout the layer;
- a configuration governed by local charge neutrality at the expense of the mixing entropy of counterions, i.e., the repulsive particle-gel interaction is a result of the entropic cost and local charges arising upon compression of the layer;
- the system resides below the Manning condensation threshold, where counterions are essentially free and thus considered as ideal gas of concentration Nc .

Using this approach, the disjoining pressure is given by an osmotic pressure $p = k_B T N c^*$, where the monomer density in the presence of salt, $c^* = \nu c^2$, is rescaled due to the smaller amount of counterions around the polyelectrolyte. The scaling factor $\nu \approx 4\pi b \kappa^{-2}$ is the effective excluded volume per monomer, with the modified Debye screening length, $\kappa^{-1} = 1/(4\pi b (c + 2n_s))^{1/2}$, the Bjerrum length, $b = (e^2/(4k_B T \epsilon_0 \epsilon_r)) = 0.72$ nm, and the salt concentration, n_s . Taking the monomer surface density, Γ together with the above expressions, the interaction potential of the polyelectrolyte layer $V_{\text{pol}}(\Delta h)$ and its second derivative $V''_{\text{pol}}(\Delta h)$ are obtained by integration of $p/k_B T$ over the interacting particle-hydrogel surface (Pincus model, PinM):

$$\begin{aligned} \frac{V_{\text{pol}}(\Delta h)}{k_B T} &\approx \frac{\pi R \Gamma}{n_s} \left[\Gamma \ln \left(\frac{\Gamma + 2n_s h_0}{\Gamma + 2n_s (\Delta h + h_0)} \right) + 2n_s (\Delta h + h_0) \right. \\ &\quad \left. \ln \left(\frac{(\Delta h + h_0) (\Gamma + 2n_s h_0)}{h_0 (\Gamma + 2n_s (\Delta h + h_0))} \right) \right] \text{ and } \frac{V''_{\text{pol}}(\Delta h)}{k_B T} \\ &\approx \frac{2\pi R \Gamma^2}{(\Delta h + h_0) (\Gamma + 2n_s (\Delta h + h_0))} \end{aligned} \quad (4)$$

h_0 is the equilibrium hydrogel layer thickness and $h_0 + \Delta h$ denotes the interspace between glass substrate and particle. The second model by Ross and Pincus takes into account the high salt concentration regime, where the electrostatic excluded volume is reduced due to the decreasing number of counterions. In this case integration of $p/k_B T$ over the interacting surface (Ross and Pincus model, RoPinM)⁴⁵ yields

$$\begin{aligned} \frac{V_{\text{pol}}(\Delta h)}{k_B T} &\approx \frac{\pi R a^2 \Gamma^2}{\sqrt{8\pi b n_s}} \left[\ln \left(\frac{h_0}{(\Delta h + h_0)} \right) + \frac{\Delta h}{h_0} \right] \text{ and } \frac{V''_{\text{pol}}(\Delta h)}{k_B T} \\ &\approx \frac{\pi R a^2 \Gamma^2}{\sqrt{8\pi b n_s}} \frac{1}{(\Delta h + h_0)^2} \end{aligned} \quad (5)$$

Note that in contrast to simple interfaces where counterions generate an exponential screening law, the disjoining pressure in polyelectrolytes decays only with an algebraic power law of the electrolyte concentration.

II. Other physical forces. Molecules are polarized into dipoles wherefore van der Waals (vdW) forces need to be considered. The surfaces of both, hydrogel and latex particle, are charged such that electrostatic forces should play a role as well. However, due to the physiological buffer solution of high ionic strength (150 mM NaCl) both of these interactions are screened to a large extent: For electrostatic forces, the remaining length scale of the interaction is given by the Debye screening length, which amounts to $\kappa^{-1} \approx 1$ nm for

the present experimental setup. Hence, this interaction can be neglected. In the case of vdW forces, we follow the traditional description by Israelachvili, considering an interaction between three parallel dielectric interfaces (glass/hydrogel/buffer/latex) immersed in a polar medium. The size of the particle justifies an approximation as nearly planar interfaces,⁴⁶ and in this configuration, the vdW-interaction reads:

$$V_{\text{vdW}}(\Delta h) = -\frac{A_{\text{H}}R}{12\pi} \left[\frac{1}{(\Delta h + h_0)} - \frac{1}{\Delta h} \right] \quad (6)$$

The Hamaker constant A_{H} for dielectrics immersed in aqueous solution is on the order of $1-4 k_{\text{B}}T$. As described by Mahanty and Ninham,⁴⁷ A_{H} is frequency dependent, but for interactions across an electrolyte, screening effects drastically reduce the zero-frequency part and the Hamaker constant becomes $A_{\text{H}}(\nu) = 2\kappa\Delta h \times \exp(-2\kappa\Delta h) \times A_{\text{H}}(\nu = 0) + A_{\text{H}}(\nu > 0)$. Knowing the dielectric permittivities and refractive indices of the different layers, we calculated $A_{\text{H}}(\nu = 0) \sim 0$ and $A(\nu > 0) = 8 \times 10^{-21} \text{ J}$.⁴⁶

Another repulsive interaction arises from the hydrodynamic pressure in the interstitial fluid between the fluctuating particle and the hydrogel.^{48,49} It generates a frictional (lubrication) force, which was described by Zhang et al.⁴⁹ for colliding particles:

$$V_{\text{lub}}(\Delta h) = -\frac{\pi\eta\nu R^2}{2l_0} [(\Delta h \times \ln(\Delta h) - \Delta h) - \ln(6l_0) \times \Delta h] \quad (7)$$

Here, the settling velocity ν of the particle approaching the wall, $\nu \approx 1(\mu\text{m}/\text{s})$, is easily calculated from the balance of drag forces and buoyant forces acting on the particle. l_0 is the mean free path of water molecules, being 42 nm for 1 atm.

The last relevant contribution to the particle-substrate interaction arises from gravitation, whose potential is given by $V_{\text{grav}}(\Delta h) = ((4\pi)/3) \Delta\rho gR^3\langle\Delta h\rangle$. (8) The density difference is $\Delta\rho = \rho_{\text{latex}} - \rho_{\text{buffer}} = 0.05(\text{g}/\text{cm}^3)$ and $g = 9.81 \text{ m}/\text{s}^2$ is the gravitational acceleration.

In total, the particle-substrate interaction potential consists of a direct superposition of two attractive and two repulsive contributions:

$$V(\Delta h) = V_{\text{pol}}(\Delta h) + V_{\text{grav}}(\Delta h) + V_{\text{vdW}}(\Delta h) + V_{\text{lub}}(\Delta h) \quad (9)$$

AFM Studies. The surface elasticity of the triblock copolymer hydrogel films was determined from force-indentation curves using an AFM⁵⁰ (NanoWizard, JPK instruments, Berlin, Germany). The commercial silicon-nitride cantilever had a spring constant of 15 mN/m and was equipped with a half-pyramidal tip (Veeco Instruments, Mannheim, Germany). Prior to hydrogel indentation experiments, the cantilever spring constant was calibrated measuring the thermally induced motion of the unloaded cantilever. The frequency of the tip approach/retract cycle was set to 1 Hz. One hour before starting the measurement, substrates were immersed in HEPES buffer at specific pH. During the measurement 10 positions distributed over the sample were recorded.

Young's moduli, E , of the hydrogel were determined fitting the force-indentation curves using Sneddon's modification of the Hertz model:⁵¹ $F = ((2\tan(\beta))/\pi)(E/(1-\mu^2))\delta^2$, where F is the load, δ the indentation depth, μ the Poisson ratio, and β a semivertical angle of the indenter. In this study, μ and β were assumed to be 0.5° and 35° , respectively. Fitting of force-indentation data yielded the elastic modulus E .

RESULTS AND DISCUSSION

Figure 3A shows typical results of the particle fluctuation distribution on hydrogel substrates at different pH. To provide a fair impression of typical data, three different results are shown per condition (for higher number of data sets images were too crowded). The negative logarithm of height distributions, $-\ln(P(\Delta h))$, which is proportional to the interaction potential $V(\Delta h)$ (see eq 3), exhibits a parabolic shape, which justifies the imposed harmonic approximation of

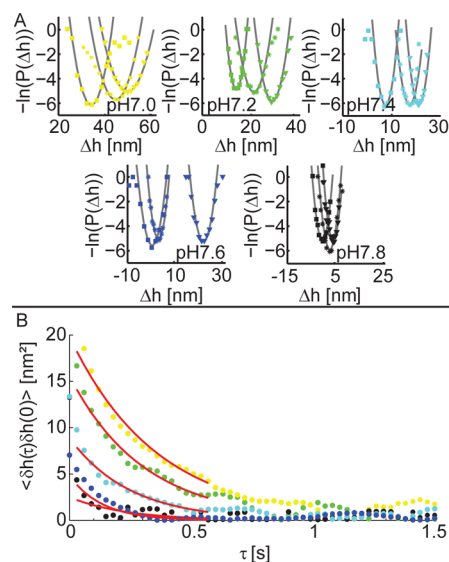


Figure 3. (A) Typical examples of the height distribution function $-\ln(P(\Delta h))$ at different pH. The negative logarithm yields a parabolic distribution, which reflects the particle-substrate interaction potential $V(\Delta h)$ eq 3. From the parabolic fit, V'' and $\langle\Delta h\rangle$ are extracted. With higher pH, parabolas are stretched and shifted toward lower heights. (B) Representative plots of the temporal hACF of fluctuations (color code as in (A)). The initial decay is fitted with a single exponential decay (eq 2 red line).

$V(\Delta h)$ according to Derjaguin.⁴² With increasing pH, the parabola is stretched and its minimum shifted toward smaller heights. The parabolic curvature, V'' , can be interpreted as the sharpness of the potential confinement, like a “spring constant”, which reflects the elasticity of the underlying material. Since the increase in pH leads to the decrease in intermicellar repulsions (Figure 1), our experimental finding reflects the compaction of the hydrogel at elevated pH. Table 1 gives an overview of the average parameter values obtained from the parabolic fits to at least 15 particles per condition. This summary shows that the average height decreases and V'' increases from 10^{-22} to $10^{-21} \text{ J}/\text{nm}^2$ with increasing pH.

The hACF of fluctuations (Figure 3B) exhibits a single exponential decay and was fitted with eq 2. According to the increase in pH from 7.0 to 7.8, the mean square fluctuation amplitude, $\langle\delta h^2(0)\rangle$, and relaxation time, τ_c , decreased by a factor of ~ 4 and ~ 2 , respectively.

The decrease in mean square fluctuation amplitude $\langle\delta h^2(0)\rangle$ indicates the damping of vertical Brownian motion, which is also reflected by the increase in V'' . However, the relaxation time τ_c is a direct measure of the dissipative hydrodynamic force, which can be used to calculate η_{eff} by eq 2 together with the Reynolds formula for the friction coefficient:⁵² $\gamma = 6\pi\eta_{\text{eff}}(R^2/\langle\Delta h\rangle)$. It was found that η_{eff} decreases with increasing pH, which could be understood because η_{eff} exceeds the viscosity of the bulk solution ($\eta = 1 \text{ mPas}$; see Table 1) due to changes in the degree of hydration.

Modulation of Interfacial Interaction Potentials by Polymer-Induced Forces. To test the validity of polyelectrolyte description $-\ln(P(\Delta h))$ data were fitted with $V(\Delta h)$, where polyelectrolyte forces were represented either by PinM eq 4) or RoPinM (eq 5). Since the parameters R , T , A_{H} , h_0 , n_{sv} , ρ_{latex} , b , and ν are either known or experimentally measurable, a fit with PinM and RoPinM yields the monomer surface density,

Table 1. Overview of System Parameters and Their Value

pH	7.0	7.2	7.4	7.6	7.8
$\langle \Delta h \rangle_t$ [nm]	35	24	17	19	4
$V'' \times 10^{-22}$ [J/nm ²]	4 ± 2	5 ± 2	8 ± 3	8 ± 2	11 ± 3
τ_c [s]	0.4 ± 0.2	0.4 ± 0.3	0.3 ± 0.2	0.3 ± 0.2	0.2 ± 0.1
η_{eff} [mPas]	2.9	2.7	1.8	1.7	0.2
PinM: $\Gamma \times 10^{15}$ [1/m ²]	17 ± 6	15 ± 5	14 ± 3	14 ± 4	5 ± 3
RoPinM: $\Gamma \times 10^{15}$ [1/m ²]	1.2 ± 0.5	0.9 ± 0.4	0.8 ± 0.3	0.9 ± 0.3	0.4 ± 0.2

Γ . For RoPinM, the effective micellar size was taken as the square monomer length $a = 68$ nm, as measured by DLS.³¹

Figure 4A shows the fits of experimentally determined $V''(\Delta h)$ with PinM (gray dashed lines) and RoPinM (red solid

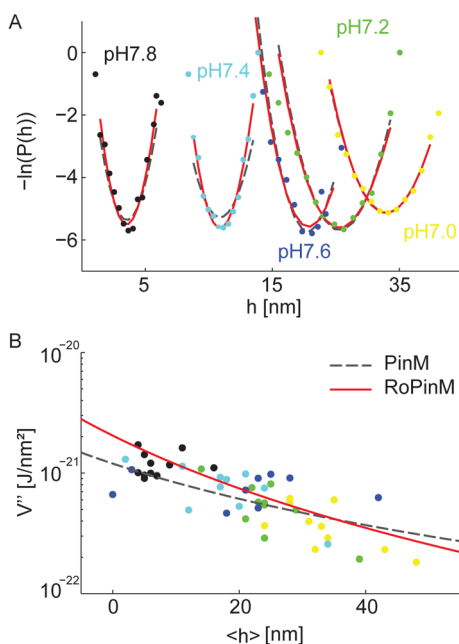


Figure 4. (A) $-\ln(P(h))$ at pH 7 (yellow), 7.2 (green), 7.4 (cyan), 7.6 (blue), and 7.8 (black). According to the increase in pH, $\langle \Delta h \rangle$ shifts toward smaller values. Models of the interaction potential, consisting of a gravitational and a polyelectrolyte induced potential, are fitted to the parabolic shape. Fitting results corresponding to PinM (gray dashed line) and RoPinM (red line) were presented for comparison. (B) Plot of V'' versus $\langle \Delta h \rangle$ of the particle above the substrate. Lines represent the calculated polyelectrolyte repulsion with parameter values obtained from the fits in (A), where $a = 68$ nm, $\Gamma = 0.8 \times 10^{15}$ 1/m², $n_s = 0.08$ 1/nm³, and $b = 0.72$ nm.

line). Here, the RoPinM yields reasonable agreement with data (Table 2) and slightly better χ^2 values close to 1. In fact, fitting of RoPinM yields $\Gamma \approx 0.4 \times 10^{15}$ 1/m² at pH 8, which agrees well with the surface density of micelles 0.2×10^{15} 1/m², calculated from the effective micellar size determined by DLS at pH 8 ($a = 68$ nm).^{31,53} With an average of $\Gamma = 0.8 \times 10^{15}$ 1/m² from fitting individual $-\ln(P(\Delta h))$ curves (Figure 3A) as well

Table 2. Reduced χ^2 -Value Calculated for $-\ln(P(\Delta h))$ Fitted with $V(\Delta h) \equiv y_{\text{fit}}$ for RoPinM or PinM^a

pH	7.0	7.2	7.4	7.6	7.8
RoPinM: χ^2	0.7	1.1	1.9	1.9	1.1
PinM: χ^2	1.4	0.9	2.7	2.1	1.7

^a χ^2 -values are averages over all data sets per condition.

as the overall V'' versus $\langle \Delta h \rangle$ (Figure 4B) the RoPinM yields a more coherent description of the hydrogel behavior compared to the PinM.

Modulation of Polymer Elasticity. The above microscopic approach describes the interaction potential $V(\Delta h)$ by a superposition of nonspecific intermolecular forces and does not take any deformation of the hydrogel layer or particle into account. In a macroscopic approach, the elastic deformation of two objects under an external force is given by the so-called Hertz model.⁵¹ The particle creates a deformation of the polymer film of depth Δh due to the gravitational force F_{grav} . If one assumes the Poisson ratio of gels to be $\mu = 0.5$ and that the bulk elastic modulus of a latex particle E_{particle} (typically on the order of magnitude of 1 GPa) is much higher than that of gels E_{gel} (order of magnitude of some tens of kPa), F_{grav} can be related to Δh :^{54,55}

$$\Delta h = \left(\frac{9}{16} \frac{F_{\text{grav}}}{E_{\text{gel}}} \right)^{2/3} R^{-1/3} \quad (7)$$

Integrating the indentation force over the depth Δh yields the deformation energy $V(\Delta h)_{\text{elastic}} = (32/45)E\sqrt{R} \times \Delta h^{5/2}$. The elastic restoring force of the polymer film can harmonically be approximated for small indentation forces, exactly as in the microscopic approach: $V(\Delta h)_{\text{elastic}} = (V''/2)\Delta h^2$. Since restoring and indentation energies balance each other, the spring constant of the harmonic potential $V''(\Delta h)$ can be related to E_{gel} .

$$E_{\text{gel}} = \frac{45}{64} V'' \sqrt{R} \times \Delta h \approx 0.55 \times \frac{V''^{3/2}}{\sqrt{R}} \quad (8)$$

For example, $V'' \approx 10^{-22}$ J/nm² calculated from RICM results could be converted to $E_{\text{gel}} \approx 10$ kPa. Figure 5A illustrates typical force-indentation curves measured with AFM using conical tips (radius $r \approx 30$ nm). As presented in Figure 5B and Table 3, E_{gel} values calculated from the height fluctuation of cell-sized particles agrees well with those obtained from AFM nanoindentation measurements using sharp tips.

It should be noted that E_{gel} values determined by the height fluctuation analysis are lower than those obtained with AFM. This tendency is more pronounced at higher pH, suggesting an overestimation of fluctuation amplitudes on stiff gels, where the shot noise of the camera may afflict the relative height values stronger. Despite of slight deviations, the obtained results demonstrated that the reversible changes in bulk elastic modulus by pH modulation result in distinct changes of interfacial potentials between cells and hydrogel substrates. The stiffness values obtained also cover a wide range of elasticities found in the human body (e.g., brain: 0.1–1 kPa, skeletal muscle: 8–17 kPa and precalcified bone: 25–40 kPa), which underlines the suitability of such hydrogels for biomedical applications.

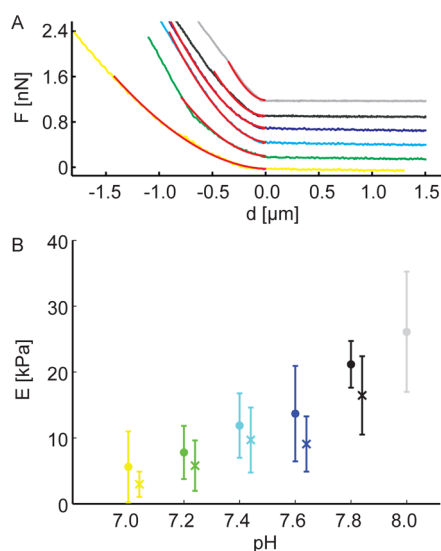


Figure 5. (A) Typical force–indentation measurements of polymer hydrogels at pH 7.0 (yellow), 7.2 (green), 7.4 (cyan), 7.6 (blue), 7.8 (black), and 8.0 (gray). Traces are shifted by an offset +0.3 nN for clarity. (B) Overview of hydrogel elasticities measured with AFM (points) and Colloidal Probe Technique (crosses). The Young modulus E of the polymer hydrogel exhibits a near linear increase with increasing pH.

CONCLUSIONS

As a simple model of generic interactions between cells and hydrogels, we investigated the net interaction between cell-sized latex particles and a pH-responsive PDDA₅₀-PMPC₂₅₀-PDDA₅₀ triblock copolymer hydrogel. The temporal fluctuation in height (i.e., vertical Brownian motion normal to the gel surface) of the latex particle was recorded using RICM, yielding the overall interfacial potential within a harmonic approximation. The systematic increase in $V''(\Delta h)$ on varying the gel pH from 7 to 8 was related to the bulk elastic modulus.

The average position of the latex particle at equilibrium is governed by the balance between gravitation, lubrication, van der Waals interaction, and polyelectrolyte-induced forces. The global shape of the reduced interfacial potentials, $-\ln P(\Delta h)$, as well as their second derivatives, $V''(\Delta h)$, are well represented by the polymer forces described by Pincus and Ross. Moreover, the surface density of monomer repeat units, Γ , estimated from the model is in excellent agreement with the value calculated from the micelle dimensions using DLS. Moreover, the bulk elastic modulus E_{gel} calculated from the second derivative of the surface potential $V''(\Delta h)$ was in reasonable agreement with the corresponding values obtained from AFM nanoindentation. These findings suggest that pH modulation does not only alter the bulk elastic modulus, but also the interfacial properties between cell-sized objects and hydrogels. An interesting extension of this study addresses the response of a mammalian cell with respect to changes in the interaction potential of the substrate. In order to investigate the cell adhesion area on such hydrogel substrates, an advanced confocal RICM needs to be

used, which overcomes the poor contrast of the conventional setup.⁵⁶ Moreover, as the modest pH modulation experienced by the hydrogel does not adversely affect cell viability,²⁹ such adjustable biocompatible interfaces suggest the possibility to further modify the microenvironment of biological cells via external stimuli.

ASSOCIATED CONTENT

Supporting Information

Supporting Information is available for (1) synthesis of triblock copolymers, (2) precision of height determination, (3) reduced χ^2 definition, and (4) derivation of the hACF. The Supporting Information is available free of charge on the ACS Publications website at DOI: 10.1021/acs.langmuir.5b01896.

AUTHOR INFORMATION

Corresponding Author

*E-mail: tanaka@uni-heidelberg.de (M.T.).

Present Address

¹Laboratoire Physico-Chimie, Institut Curie, CNRS UMR168, 75005 Paris, France

Author Contributions

M.T. conceived and directed the project. C.M. performed experiments and analyzed the results. C.M., M.T., A.L.L., and S.P.A. wrote the paper.

Notes

The authors declare no competing financial interest.

ACKNOWLEDGMENTS

M.T. thanks the support by the German Science Foundation (SFB 873 B07), Sumitomo Foundation, MEXT (No. 26103521), and JSPS (No. 26247070). S.P.A. thanks EPSRC for a Platform grant EP/J007846/1. M.T. is a member of the German Excellence Cluster “CellNetworks”. C.M. is grateful for the postdoc fellowship of CellNetworks and financial support by “Fonds der Chemischen Industrie”.

ABBREVIATIONS

PMPC, poly-2-methacryloyloxyethyl phosphorylcholine; PDDA, poly-2-(diisopropylamino)ethyl methacrylate; RICM, Reflection-Interference-Contrast-Microscopy; AFM, atomic force microscopy

REFERENCES

- (1) de Las Heras Alarcon, C.; Pennadam, S.; Alexander, C. Stimuli responsive polymers for biomedical applications. *Chem. Soc. Rev.* **2005**, *34* (3), 276–285.
- (2) Grubbs, R. B.; Sun, Z. Shape-changing polymer assemblies. *Chem. Soc. Rev.* **2013**, *42* (17), 7436–45.
- (3) Ge, Z.; Liu, S. Functional block copolymer assemblies responsive to tumor and intracellular microenvironments for site-specific drug delivery and enhanced imaging performance. *Chem. Soc. Rev.* **2013**, *42* (17), 7289–325.
- (4) Rodriguez-Hernandez, J.; Lecommandoux, S. Reversible inside-out micellization of pH-responsive and water-soluble vesicles based on

Table 3. Hydrogel Elastic Modulus Measured with AFM and Colloidal Probe Technique

pH	7.0	7.2	7.4	7.6	7.8	8.0
$E_{\text{Coll. Probe Tech.}}$ [kPa]	3 ± 2	5 ± 3	10 ± 5	9 ± 4	14 ± 5	
E_{AFM} [kPa]	6 ± 5	8 ± 4	12 ± 5	14 ± 7	21 ± 4	26 ± 9

- polypeptide diblock copolymers. *J. Am. Chem. Soc.* **2005**, *127* (7), 2026–7.
- (5) Jeong, B.; Gutowska, A. Lessons from nature: stimuli-responsive polymers and their biomedical applications. *Trends Biotechnol.* **2002**, *20*, 305–306.
- (6) Auras, R.; Lim, L.-T.; Selke, S. E.; Tsuji, H. 3. Industrial Production of High Molecular Weight Poly(Lactic Acid). In *Poly(Lactic Acid): Synthesis, Structures, Properties, Processing, and Applications*; John Wiley & Sons, Inc.: Hoboken, NJ, 2010.
- (7) Engler, A. J.; Sen, S.; Sweeney, H. L.; Discher, D. E. Matrix elasticity directs stem cell lineage specification. *Cell* **2006**, *126*, 677–689.
- (8) Nakaya, T.; Li, Y.-J. Phospholipid polymers. *Prog. Polym. Sci.* **1999**, *24*, 143–181.
- (9) Hoffman, A. S. Hydrogels for biomedical applications. *Adv. Drug Delivery Rev.* **2012**, *64*, 18–23.
- (10) Lim, F.; Sun, A. M. Microencapsulated islets as bioartificial pancreas. *Science* **1980**, *210*, 908–910.
- (11) Burdick, J. A.; Murphy, W. L. Moving from static to dynamic complexity in hydrogel design. *Nat. Commun.* **2012**, *3*, 1269.
- (12) Nishida, K.; Yamato, M.; Hayashida, Y.; Watanabe, K.; Yamamoto, K.; Adachi, E.; Nagai, S.; Kikuchi, A.; Maeda, N.; Watanabe, H.; Okano, T.; Tano, Y. Corneal reconstruction with tissue-engineered cell sheets composed of autologous oral mucosal epithelium. *N. Engl. J. Med.* **2004**, *351* (12), 1187–96.
- (13) Okano, T.; Yamada, N.; Okuhara, M.; Sakai, H.; Sakurai, Y. Mechanism of cell detachment from temperature-modulated, hydrophilic-hydrophobic polymer surfaces. *Biomaterials* **1995**, *16* (4), 297–303.
- (14) DeForest, C. A.; Anseth, K. S. Cytocompatible click-based hydrogels with dynamically tunable properties through orthogonal photoconjugation and photocleavage reactions. *Nat. Chem.* **2011**, *3* (12), 925–31.
- (15) Zhao, Y.; Liu, B.; Pan, L.; Yu, G. 3D nanostructured conductive polymer hydrogels for high-performance electrochemical devices. *Energy Environ. Sci.* **2013**, *6*, 2856–2870.
- (16) Discher, D. E.; Mooney, D. J.; Zandstra, P. W. Growth factors, matrices, and forces combine and control stem cells. *Science* **2009**, *324*, 1673–1677.
- (17) Vogel, V.; Sheetz, M. Local force and geometry sensing regulate cell functions. *Nat. Rev. Mol. Cell Biol.* **2006**, *7* (4), 265–75.
- (18) Simmons, C. A.; Alsberg, E.; Hsiong, S.; Kim, W. J.; Mooney, D. J. Dual growth factor delivery and controlled scaffold degradation enhance in vivo bone formation by transplanted bone marrow stromal cells. *Bone* **2004**, *35* (2), 562–9.
- (19) Wells, R. G. The role of matrix stiffness in regulating cell behavior. *Hepatology* **2008**, *47* (4), 1394–400.
- (20) Wolf, K.; Mazo, I.; Leung, H.; Engelke, K.; von Andrian, U. H.; Deryugina, E. I.; Strongin, A. Y.; Bocker, E. B.; Friedl, P. Compensation mechanism in tumor cell migration: mesenchymal-amoeboid transition after blocking of pericellular proteolysis. *J. Cell Biol.* **2003**, *160* (2), 267–77.
- (21) Engler, A.; Bacakova, L.; Newman, C.; Hategan, A.; Griffin, M.; Discher, D. Substrate compliance versus ligand density in cell on gel responses. *Biophys. J.* **2004**, *86* (1), 617–628.
- (22) Engler, A. J.; Griffin, M. A.; Sen, S.; Bonnemann, C. G.; Sweeney, H. L.; Discher, D. E. Myotubes differentiate optimally on substrates with tissue-like stiffness: pathological implications for soft or stiff microenvironments. *J. Cell Biol.* **2004**, *166* (6), 877–887.
- (23) Georges, P. C.; Miller, W. J.; Meaney, D. F.; Sawyer, E. S.; Janmey, P. A. Matrices with compliance comparable to that of brain tissue select neuronal over glial growth in mixed cortical cultures. *Biophys. J.* **2006**, *90* (8), 3012–8.
- (24) Lo, C. M.; Wang, H. B.; Dembo, M.; Wang, Y. L. Cell movement is guided by the rigidity of the substrate. *Biophys. J.* **2000**, *79* (1), 144–52.
- (25) Gray, D. S.; Tien, J.; Chen, C. S. Repositioning of cells by mechanotaxis on surfaces with micropatterned Young's modulus. *J. Biomed. Mater. Res.* **2003**, *66* (3), 605–614.
- (26) Shu, X. Z.; Liu, Y.; Luo, Y.; Roberts, M. C.; Prestwich, G. D. Disulfide cross-linked hyaluronan hydrogels. *Biomacromolecules* **2002**, *3* (6), 1304–11.
- (27) Engler, A. J.; Rehfeldt, F.; Sen, S.; Discher, D. E. Microtissue elasticity: measurements by atomic force microscopy and its influence on cell differentiation. *Methods in cell biology* **2007**, *83*, 521–545.
- (28) Shu, X. Z.; Ahmad, S.; Liu, Y.; Prestwich, G. D. Synthesis and evaluation of injectable, in situ crosslinkable synthetic extracellular matrices for tissue engineering. *J. Biomed. Mater. Res., Part A* **2006**, *79* (4), 902–912.
- (29) Yoshikawa, H. Y.; Rossetti, F. F.; Kaufmann, S.; Kaindl, T.; Madsen, J.; Engel, U.; Lewis, A. L.; Armes, S. P.; Tanaka, M. Quantitative evaluation of mechanosensing of cells on dynamically tunable hydrogels. *J. Am. Chem. Soc.* **2011**, *133*, 1367–1374.
- (30) Lobb, E. J.; Ma, I.; Billingham, N. C.; Armes, S. P.; Lewis, A. L. Facile synthesis of well-defined, biocompatible phosphorylcholine-based methacrylate copolymers via atom transfer radical polymerization at 20 degrees C. *J. Am. Chem. Soc.* **2001**, *123*, 7913–7914.
- (31) Ma, Y.; Tang, Y.; Billingham, N. C.; Armes, S. P.; Lewis, A. L. Synthesis of biocompatible, stimuli-responsive, physical gels based on ABA triblock copolymers. *Biomacromolecules* **2003**, *4*, 864–868.
- (32) Madsen, J.; Armes, S. P.; Bertal, K.; Lomas, H.; Macneil, S.; Lewis, A. L. Biocompatible wound dressings based on chemically degradable triblock copolymer hydrogels. *Biomacromolecules* **2008**, *9*, 2265–2275.
- (33) Ma, I. Y.; Lobb, E. J.; Billingham, N. C.; Armes, S. P.; Lewis, A. L.; Lloyd, A. W.; Salvage, J. Synthesis of Biocompatible Polymers. I. Homopolymerization of 2-Methacryloyloxyethyl Phosphorylcholine via ATRP in Protic Solvents: An Optimization Study. *Macromolecules* **2002**, *35*, 9306–9314.
- (34) Kern, W. H.; Dermer, G. B.; Tiemann, R. M. Comparative morphology of histiocytes from various organ systems. Quantitative cytologic and ultrastructural studies. *Acta Cytol.* **1970**, *14*, 205–215.
- (35) Limozin, L.; Sengupta, K. Quantitative reflection interference contrast microscopy (RICM) in soft matter and cell adhesion. *ChemPhysChem* **2009**, *10*, 2752–2768.
- (36) Monzel, C.; Fenz, S. F.; Merkel, R.; Sengupta, K. Probing biomembrane dynamics by dual-wavelength reflection interference contrast microscopy. *ChemPhysChem* **2009**, *10* (16), 2828–2838.
- (37) Fielding, L. A.; Edmondson, S.; Armes, S. P. Biocompatible polymer brushes grown from model quartz fibres: synthesis, characterisation and in situ determination of frictional coefficient. *J. Mater. Chem.* **2011**, *21*, 11773–11780.
- (38) Morse, A. J.; Edmondson, S.; Dupin, D.; Armes, S. P.; Zhang, Z.; Leggett, G. J.; Thompson, R. L.; Lewis, A. L. Biocompatible polymer brushes grown from model quartz fibres: synthesis, characterisation and in situ determination of frictional coefficient. *Soft Matter* **2010**, *6*, 1571–1579.
- (39) Albersdörfer, A. *Über das Quellverhalten und die viskoelastischen Eigenschaften ultradünner, festkörpergestützter Polyelektrolytfilme*. Dissertation; Herbert Utz Verlag, München, 1999.
- (40) Fukumoto, K.; Konishi, H.; Soga, K.; Miyawaki, K.; Okano, H.; Minami, M.; Wakabayashi, N.; Mitsufuji, S.; Yoshida, N.; Takagi, T.; Yagi, N.; Naito, Y.; Kataoka, K.; Yoshikawa, T. Successful endoscopic injection sclerotherapy of high-risk gastroesophageal varices in a cirrhotic patient with hemophilia A. *Gastroenterology research and practice* **2010**, *2010*, 518260.
- (41) Rädler, J. O.; Sackmann, E. On the measurement of weak repulsive and frictional colloidal forces by reflection interference contrast microscopy. *Langmuir* **1992**, *3*, 848–853.
- (42) Derjaguin, B. V.; Churaev, N. V. *Surface Forces*; Consultants Bureau: New York: 1987.
- (43) Prieve, D. C.; Bike, S. G.; Frej, N. A. Brownian motion of a single microscopic sphere in a colloidal force field. *Faraday Discuss. Chem. Soc.* **1990**, *90*, 209–222.
- (44) Pincus, P. Colloid Stabilization with Grafted Polyelectrolytes. *Macromolecules* **1991**, *24*, 2912–2919.
- (45) Ross, R. S.; Pincus, P. The polyelectrolyte brush: poor solvent. *Macromolecules* **1992**, *25*, 2177–2183.

- (46) Israelachvili, J. N. *Intermolecular and Surface Forces*, 3rd ed.; Academic Press: Waltham, 1991.
- (47) Mahanty, J.; Ninham, B. W. *Dispersion Forces*; Academic Press: London, 1976.
- (48) Leikin, S.; Parsegian, V. A.; Rau, D. C.; Rand, R. P. Hydration forces. *Annu. Rev. Phys. Chem.* **1993**, *44*, 369–95.
- (49) Zhang, W.; Noda, R.; Horio, M. Evaluation of lubrication force on colliding particles for DEM simulation of fluidized beds. *Powder Technol.* **2005**, *158*, 92–101.
- (50) Landman, U.; Luedtke, W. D.; Burnham, N. A.; Colton, R. J. Atomistic mechanisms and dynamics of adhesion, nanoindentation, and fracture. *Science* **1990**, *248* (4954), 454–61.
- (51) Hertz, H. Über die Berührung fester elastischer Körper. *J. Reine Angew. Math.* **1881**, *92*, 156–171.
- (52) Reynolds, O. On the theory of Lubrication and its Application to Mr. Beauchamp Tower's Experiments, including an Experimental Determination of the Viscosity of Olive Oil. *Philos. Trans. R. Soc. London* **1886**, *177*, 157–177.
- (53) Castelletto, V.; Hamley, I. W.; Ma, Y.; Bories-Azeau, X.; Armes, S. P.; Lewis, A. L. Microstructure and physical properties of a pH-responsive gel based on a novel biocompatible ABA-type triblock copolymer. *Langmuir* **2004**, *20*, 4306–4309.
- (54) Landau, L. D.; Lifshitz, E. M. *Theory of Elasticity*; Pergamon Press Inc.: New York, 1986.
- (55) Sengupta, K.; Schilling, J.; Marx, S.; Fischer, M.; Bacher, A.; Sackmann, E. Mimicking Tissue Surfaces by Supported Membrane Coupled Ultrathin Layer of Hyaluronic Acid. *Langmuir* **2003**, *19*, 1775–1781.
- (56) Matsuzaki, T.; Sazaki, G.; Suganuma, M.; Watanabe, T.; Yamazaki, T.; Tanaka, M.; Nakabayashi, S.; Yoshikawa, H. Y. High Contrast Visualization of Cell–Hydrogel Contact by Advanced Interferometric Optical Microscopy. *J. Phys. Chem. Lett.* **2014**, *5* (1), 253–257.